ACS SyntheticBiology
Cite This: ACS Synth. Biol. XXXX, XXX, XXX−XXX
Letter
pubs.acs.org/synthbio

Low-Burden Biological Feedback Controllers for Near-Perfect Adaptation

Harrison Steel* and Antonis Papachristodoulou*

Dept of Engineering Science, University of Oxford, Oxford OX1 3PJ, U.K.

Supporting Information

ABSTRACT: The robustness and reliability of synthetic biological systems can be substantially improved by the introduction of feedback control architectures that parallel those employed in traditional engineering disciplines. One common control goal is adaptation (or disturbance rejection), which refers to a system's ability to maintain a constant output despite variation in some of its constituent processes (as frequently occurs in noisy cellular environments) or external perturbations. In this paper, we propose and analyze a control architecture that employs integrase and excisionase proteins to invert regions of DNA and an mRNA−mRNA annihilation reaction. Combined, these components approximate the functionality of a switching controller (as employed in classical control engineering) with three distinct operational modes. We demonstrate that this system is capable of near-perfect adaptation to variation in rates of both transcription and translation and can also operate without excessive consumption of cellular resources. The system's steady-state behavior is analyzed, and limits on its operating range are derived. Deterministic simulations of its dynamics are presented and are then extended to the stochastic case, which treats biochemical reactions as discrete events.

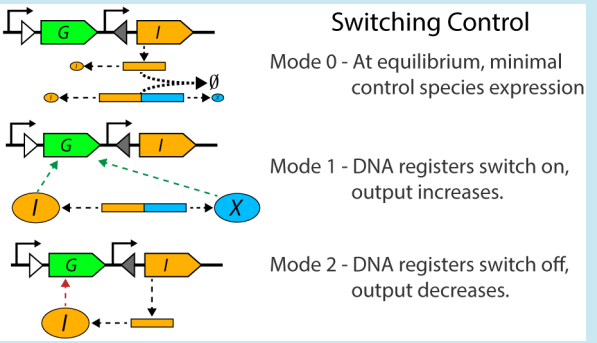

KEYWORDS: *synthetic biology, biological control, adaptation, switching controller, recombinase enzymes*

Recent work in synthetic biological research has focused on the development of control architectures that parallel those employed in other engineering disciplines,[1,2] with the aim of improving the robustness and reliability of engineered biological systems.[3] A central goal of this work has been the creation of biological systems capable of *adaptation* (e.g., to achieve disturbance rejection). This can be loosely defined as the ability of a system to maintain one variable's value (for example, the concentration of a biochemical species) constant as the parameters or behavior of a system with which it interacts varies. Adaptation has been observed to occur in some natural systems,[4,5] structural design constraints that must be satisfied to achieve this functionality have been outlined,[6,7] and control architectures that achieve near-perfect adaptation have recently been experimentally demonstrated.[8] Similar feedback circuits have also been created using a range of biological components, such as synthetic protein scaffolds[9] and sigma/antisigma factors.[8,10] However, at present, these implementations struggle to overcome challenges such as leakiness of their "integrator" components (which are required for perfect adaptation) because of dilution/degradation of their constitutent components.[11,12] This has led to the proposition of alternative approaches that, though not allowing *perfect* adaptation, nevertheless come close (for example, by employing systems that exhibit an ultrasensitive input−output mapping[13]).

In this paper, we propose and analyze a different control system that provides a range of benefits when compared to previously proposed architectures: It allows near-perfect rejection of disturbances to both cell-wide translation rates (frequently arising due to ribosome sequestration[14,15]) and transcription rate (arising due to fluctuations in plasmid copy number[16]). Furthermore, our system is designed to operate in a "slack region" where (at equilibrium) the expression rate of its constituent proteins is minimized. This reduces the burden (consumption of cellular resources) that it imparts upon its host cell, which could otherwise adversely impact cellular growth and the behavior of other synthetic circuits.[17−20]

The system proposed achieves these goals by using two biological motifs employed in recent experimental work: First, integrase/excisionase proteins (which have been used to implement information storage,[21,22] logic,[23] and feedback control[24]) are employed to flip a DNA "register" flanked by recognition sites. This aspect of our design is motivated by a desire to side-step the impact of dilution effects experienced by controllers for which internal states are stored as protein concentrations; DNA registers avoid this as their state is maintained during duplication. Second, an mRNA−mRNA annihilation reaction provides functionality similar to that of a "subtraction" junction from traditional control engineering. Biological feedback control structures that employ similar mRNA−sRNA annihilation interactions have been theoret-

Received: March 22, 2019
Published: September 9, 2019

DOI: 10.1021/acssynbio.9b00125
ACS Synth. Biol. XXXX, XXX, XXX−XXX

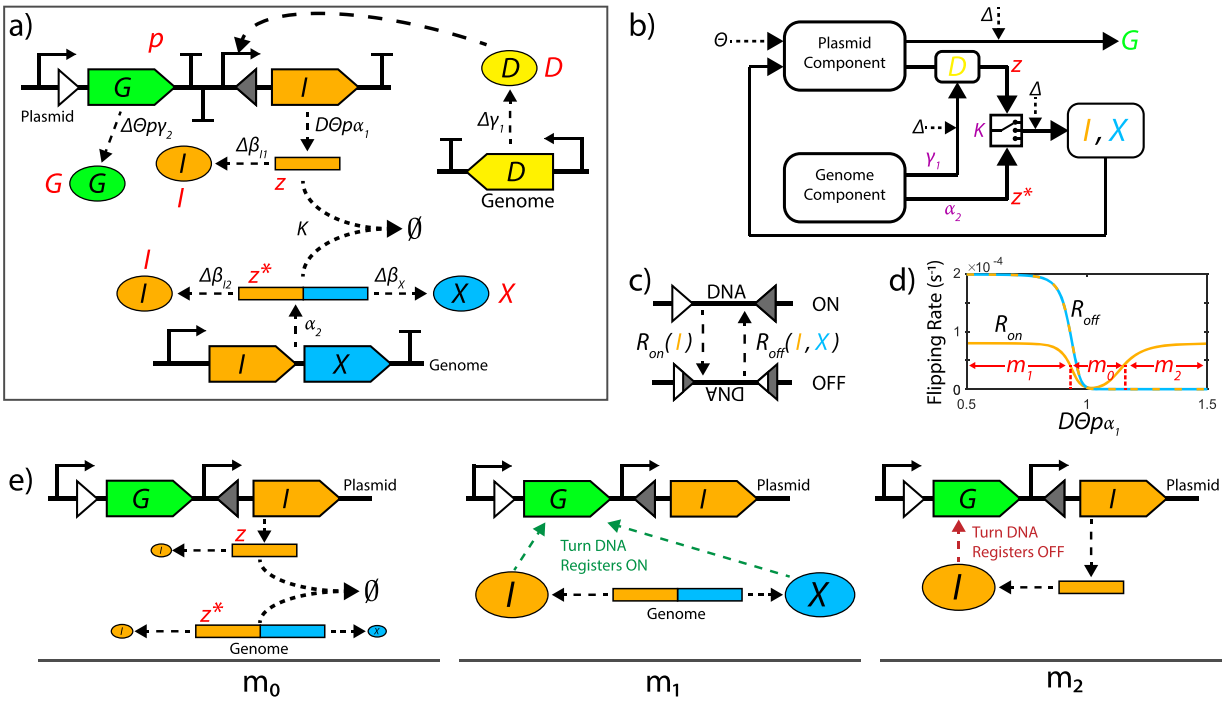

Figure 1. Proposed control architecture. (a) The integrase/excisionase control architecture proposed in this work, which is designed to reject disturbances to transcription (Θ) and translation (Δ) rates. It consists of interacting mRNA species (z, z^*) that mutually annihilate, an output protein (G), a measurement protein (D, which couples translation variation to the transcription of z), and recombinase enzymes (I, X), which flip DNA registers (flanked by converging triangles). State variables from eq 1a−g are in red, and other parameters are as described in Table 1. (b) Block diagram of the control system, including a selector junction for the system's three modes. Important parameters for tuning are highlighted in purple. (c) Illustration of integrase/excisionase mediated flipping of a DNA register between recognition sites (triangles). Solid triangles represent initial DNA recognition sites (requiring I for flipping), and half-colored triangles represent flipped DNA sites (requiring I and X for reverse flipping). (d) DNA flipping rates as a function of steady-state I and X values when the production rate of z ($D\Theta p\alpha_1$) is set to a fixed value, demonstrating a "slack region" (m_0, where $D\Theta p\alpha_1 \approx 1$), near which both flipping rates are small. (e) Illustration of the controller's three switching modes. In mode m_0, production of mRNA species z and z^* is balanced, meaning most mRNA are bound to one another (preventing translation), and thus, DNA flipping is slow. When the system is disturbed (by a change in cell-wide translation rate or plasmid copy number), mRNA production is out of balance, and the system enters either mode m_1 (to increase output G) or m_2 (to decrease G). In m_1, genome-expressed integrase and excisionase work together to flip DNA registers to their ON position, whereas in m_2, plasmid-expressed integrase flips registers to their OFF position.

ically[11,25] and experimentally[26−28] demonstrated in the literature. The novelty of the present work thus focuses on the interconnection of these two biological motifs, resulting in a controller that benefits from the useful properties of each motif. The architecture we develop is inspired by switching control schemes (commonly employed in classical control engineering[29,30]), which move between discrete operational modes depending on a reference signal.

RESULTS

System Description. In this study, we propose a biological implementation of a switching controller (Figure 1a), which aims to regulate its output G to adapt to cell-wide disturbances Δ in translation rate (which could arise due to varying ribosome availability) and Θ in transcription rate of plasmid-encoded genes (which could arise due to varying plasmid copy number). Figure 1b presents a block diagram for the system, outlining the interactions between components as well as the points at which these disturbances are introduced. Disturbance rejection is achieved by regulating the number of plasmid DNA registers in their ON position (which determines the transcription rate of the controller's output, G) via switching the controller between three operating modes (Figure 1e).

Our proposed system consists of a plasmid-encoded component (which includes a flippable DNA register and genes for the system output G and mRNA z) and a genome-encoded component (which includes mRNA z^*). Also encoded in the genome is a measurement species D, which is responsible for coupling variations in translation rate (Δ) to the expression of z. Control functionality is implemented using integrase (I) and excisionase (X) proteins that flip a DNA register flanked by recognition sites (Figure 1c), regulating the proportion of DNA registers that are in their ON position (p, which we initially treat as a continuous variable). I alone can flip DNA from ON to OFF, whereas both I and X are required for the reverse flipping operation.[24] From registers in their ON position, the output G is transcribed as is mRNA z (encoding I). Meanwhile, an mRNA z^* that encodes both I and Z is transcribed continuously from the genome as is measurement species D. The mRNAs z and z^* irreversibly bind to each other in such a way that translation from each is suppressed.

The overall design can be conceptualized as an approximation of a switching controller[29,30] that operates in three distinct modes, m_0, m_1, and m_2 (Figure 1e), defined as follows: When production rates of z and z^* are balanced, little I or X is produced, meaning flipping is slow (both R_{on} and R_{off} are small) and p remains approximately constant (mode m_0). However, the concentration of z (and G) can be disturbed by a change in either transcription rate via Θ or global translation rate via Δ (because the production of z is regulated by the measurement

DOI: 10.1021/acssynbio.9b00125
ACS Synth. Biol. XXXX, XXX, XXX−XXX

protein species D). When this inbalance in z and z^* arises, either I (if $z \gg z^*$, mode m_2) or I and X (if $z \ll z^*$, mode m_1) will be produced, which leads to flipping of DNA registers (varying p) to return expression of z and G to its desired set-point. The boundaries between different control modes are illustrated numerically in Figure 1d, where we fix the production rate of z ($D\Theta p\alpha_1$) and then calculate corresponding steady-state I and X concentrations: when $D\Theta\, p\alpha_1 \approx 1$ (mode m_0), we have R_{on}, $R_{off} \approx 0$, and so, minimal flipping occurs in either direction.

ODE Model. The proposed control system can be described using a system of ordinary differential equations (ODEs) of the form

$$\dot{D} = \Delta\gamma_1 - \delta_2 D \tag{1a}$$

$$\dot{z} = D\Theta p\alpha_1 - \delta_1 z - Kzz^* \tag{1b}$$

$$\dot{z}^* = \alpha_2 - \delta_1 z^* - Kzz^* \tag{1c}$$

$$\dot{I} = \Delta\beta_{I1} z + \Delta\beta_{I2} z^* - \delta_2 I \tag{1d}$$

$$\dot{X} = \Delta\beta_X z^* - \delta_2 X \tag{1e}$$

$$\dot{G} = \Delta\Theta p\gamma_2 - \delta_3 G \tag{1f}$$

$$\dot{p} = R_{off}(I, X)(1 - p) - R_{on}(I)(p) \tag{1g}$$

where state variables D, z, z^*, I, X, and G are concentrations as defined previously, and $p \in [0,1]$ is the proportion of registers in their "ON" state. α's are transcription rates, β's are translation rates, γ's are lumped transcription/translation rates, δ's are combined rates of degradation/dilution, and K is the binding rate between mRNAs. The parameter Δ is used to introduce disturbances in global (cell-wide) translation rate, and Θ introduces disturbances in transcription from the plasmid encoding G and z. Initially, we have $\Delta, \Theta = 1$; variation from this value represents introduction of a disturbance. Integrase/excisionase mediated DNA flipping is described by

$$R_{off}(I, X) = r_{off} f_X(X) f_I(I) \tag{2a}$$

$$R_{on}(I) = r_{on} f_I(I) \tag{2b}$$

$$f_X(X) = \frac{X^4}{K_X^4 + X^4} \tag{2c}$$

$$f_I(I) = \frac{I^4}{K_I^4 + I^4} \tag{2d}$$

where $r_{on,off}$ are scaling factors for the rates of DNA inversion, $K_{I,X}$ are equilibrium constants that determine the concentration of each protein required for the half-maximum flipping rate to be achieved, and the order four Hill functions arise due to four molecules of each protein being required (one dimer at each recognition site) to perform DNA inversion.[24,31] A summary of the model parameters is provided in Table 1, and the numerical values used in simulations are discussed in Supplementary Section 1.

Steady-State Analysis. We can solve eq 1a−g at steady state to eliminate variables D, z^*, I, and X, finding that the equilibrium concentration of z must satisfy

$$\frac{\alpha_1\gamma_1\Delta\Theta p}{\delta_2} = \delta_1 z + Kz\mu(z) \tag{3a}$$

Table 1. Summary of Model Parameters and State Variables[a]

parameter	description
Θ	transcriptional disturbance magnitude
Δ	translational disturbance magnitude
$\alpha_{1,2}$	transcription rates
$\beta_{I1,I2,X}$	translation rates
$\gamma_{1,2}$	lumped transcription/translation rate
K	mRNA−mRNA binding rate
$K_{I,X}$	integrase/excisionase equilibrium constant
$\delta_{1,2,3}$	mRNA/protein combined degradation/dilution rate
$r_{on,off}$	rates of DNA inversion
z, z^*	mRNA concentrations
G, I, X, D	protein concentrations
p	fraction of plasmids in "ON" position
$\hat{p}$	number of plasmids in "ON" position
p_T	total number of plasmids per cell

[a]For numerical values, see Table S1.

$$p = \frac{f_X(\Delta\beta_X\mu(z)/\delta_2)}{\frac{r_{on}}{r_{off}} + f_X(\Delta\beta_X\mu(z)/\delta_2)} \tag{3b}$$

$$\mu(z) = \frac{\alpha_2}{\delta_1 + Kz} \tag{3c}$$

where we note that the factor $\Delta\Theta p$ (proportional to the production rate of G) appears on the left-hand side of eq 3a. If we have $Kz \gg \delta_1$ (i.e., most mRNA binds to its complementary mRNA prior to degrading), then the right-hand side of eq 3a can be simplified to give $p\Delta\Theta \propto \delta_1 z + \alpha_2$, meaning that G will reject changes in Δ, Θ so long as $\delta_1 z$ does not vary significantly. This can be partially achieved by minimizing δ_1 (as in other biological circuits targeting adaptation[11]) as well as by minimizing the sensitivity of the steady-state value of z to changes in Δ and Θ, which we analyze in Supplementary Section 2.

This architecture's ability to reduce variation in the steady-state z value (and hence the term $\delta_1 z$) can be conceptually understood as arising from "ultrasensitive" behavior due to z entering the first term in eq 3b through the fourth-order Hill function f_X. Other biological feedback controllers have been proposed that utilize ultrasensitivity to provide similar adaptive behavior,[13] though the "ultrasensitive" component is typically implemented using a zeroth-order process (such as a balanced phosphorylation cycle) or high-cooperativity transcription factor regulation.[32] We define our system's *target* as being the steady-state value G_0, determined by eq 1a−g when $\Delta, \Theta = 1$; our control system aims to make the difference between its output and this target small for disturbances Δ and Θ, (i.e., the steady-state error $|G(\Delta, \Theta) - G_0|$).

In our previous work,[24] feedback controllers were built using integrase/excisionase proteins in order to reduce the influence of noise sources upon a circuit's output. In ref 24, the proportion of registers in their active state was (at equilibrium) maintained by continuous flipping between states (i.e., I and X were both large, and R_{on} and R_{off} were balanced). In contrast, the controller outlined herein is designed to move between different switching modes (Figure 1e), which drive its state toward a "slack region", in which integrase/excisionase concentrations are small. Thus, at (or near) its equilibrium, our controller produces little of the control species I and X, minimizing its burden upon the cell.

Performance Bounds. We can bound the controller's slack region (i.e., approximate the boundaries of m_0) by maximal concentrations of I and X, which we define as the point at which

DOI: 10.1021/acssynbio.9b00125
ACS Synth. Biol. XXXX, XXX, XXX−XXX

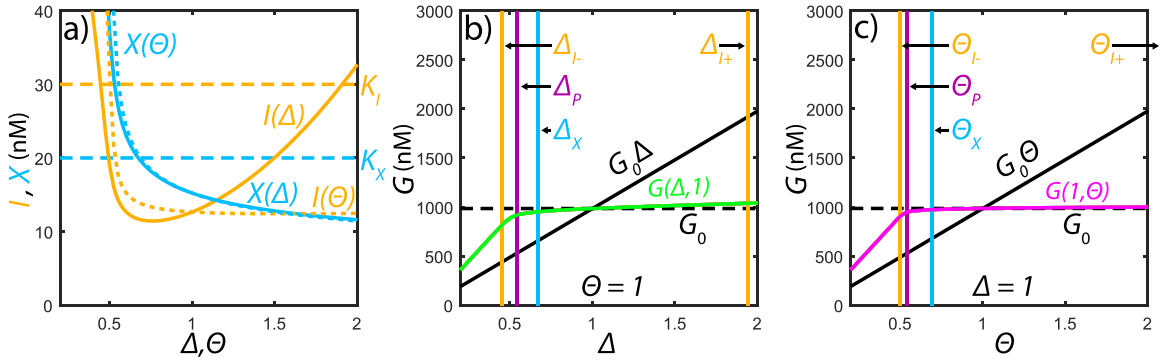

Figure 2. Steady-state analysis. (a) Steady-state I and X concentrations as a function of Δ ($I(\Delta)$ and $X(\Delta)$, solid lines, $\Theta = 1$) or Θ ($I(\Theta)$ and $X(\Theta)$, dotted lines, $\Delta = 1$). (b) System steady-state output ($G(\Delta,1)$) as a function of Δ with $\Theta = 1$, compared to its target value (G_0, black dashed line) and the result from an uncontrolled case ($G_0\Delta$). Limiting values of Δ as described in the text are indicated by vertical lines. Control capability quickly declines for Δ values below the saturation point Δ_p. (c) Similar to panel (b), but with $\Delta = 1$ and Θ varying. $\Theta_{I+} \approx 500$ is not pictured.

flipping rates are 50% of their maximum (i.e., $X = K_X$ or $I = K_I$ such that $f_X = f_I = 0.5$). In this slack region, we have $I < K_I$ and $X < K_X$, and thus, flipping occurs slowly. The system leaves this slack region (into either m_2 with $I > K_I$ or m_1 with $X > K_X$ and $I > K_I$) for only short periods of time (immediately following a change in Δ or Θ), during which fast convergence (variation in p) occurs to bring the output G back toward G_0. To assess the range of Δ or Θ values for which the system's steady state lies in this slack region, we solve eq 1c and either eq 1d or 1e for z at steady state giving

$$z_X = \frac{\Delta\alpha_2\beta_X - K_X\delta_1\delta_2}{K_X K\delta_2} \tag{4a}$$

$$z_{I+,I-} = \frac{KK_I\delta_2 - \Delta\beta_{I1}\delta_1 \pm \sqrt{s}}{2\Delta K\beta_{I1}} \tag{4b}$$

$$s = (KK_I\delta_2 + \Delta\beta_{I1}\delta_1)^2 - 4\Delta^2\alpha_2\beta_{I1}\beta_{I2}K \tag{4c}$$

and substitute these expressions into eq 3a−c. We can solve the resulting equation for Δ (with $\Theta = 1$) or Θ (with $\Delta = 1$) to yield $\Delta_{I-,I+,X}$ and $\Theta_{I-,I+,X}$ corresponding to $z_{I-,I+,X}$, respectively. This gives an acceptable range of disturbances $\max[\Delta_{I-}, \Delta_X] < \Delta < \Delta_{I+}$ (and similar for Θ). Thus, when disturbances are in this range (considering variation to Δ and Θ separately), the system's equilibrium lies in a region within which both $I < K_I$ and $X < K_X$ are at steady state. This region is illustrated in Figure 2a where steady-state I and X concentrations are plotted for varying disturbances; the various limiting values correspond to intersections between functions (e.g., $\Delta_{I-,+}$ are the Δ values at which I crosses K_I). However, because we have not considered saturation of p, we have as yet made no guarantee that these limits can actually be reached prior to controller saturation.

We can constrain the magnitude of disturbances that the control system can reject without saturating by examining its performance at limiting values of p. As Δ, Θ increase, the value of the product $\Delta\Theta p$ in eq 1f can be maintained by setting an appropriately small p. However, though the system does not run out of actuating potential in this case (i.e., we never reach $p = 0$), the steady-state error may increase. For the case where $\Delta, \Theta \to 0$, the value of $\Delta\Theta p$ can only be maintained up to the point where $z = 0$, and almost all registers are in their ON position. We can solve eq 3a−c to find the steady-state value $\hat{z}$ when $\Delta = \Theta = 1$, which we then substitute into

$$\frac{f_X(\beta_X\hat{\mu}/\delta_2)}{\frac{r_{on}}{r_{off}} + f_X(\beta_X\hat{\mu}/\delta_2)} = \Theta\Delta\frac{f_X(\Delta\beta_X\alpha_2/\delta_1\delta_2)}{\frac{r_{on}}{r_{off}} + f_X(\Delta\beta_X\alpha_2/\delta_1\delta_2)} \tag{5a}$$

$$\hat{\mu} = \frac{\alpha_2}{\delta_1 + K\hat{z}} \tag{5b}$$

in which the right-hand side of eq 5a is the saturated signal $\Delta\Theta p$ when $z = 0$. Solving eq 5a,b for Δ (with $\Theta = 1$) or Θ (when $\Delta = 1$) gives minimal values Δ_p and Θ_p, respectively, that the system could compensate for without saturating, though steady-state error will again increase as this value is approached.

In Figure 2b,c, we analytically calculate the steady-state outputs of eq 1a−g (denoted $G(\Delta, \Theta)$) over a range of Δ and Θ values. The various limiting values of Δ and Θ described previously are plotted as vertical lines as is the expected output ($G_0\Delta\Theta$) that would result without the controller's action (i.e., if G expression was independent of p). We observe that the system is able to reject a disturbance in Δ and operates in the intended "slack region" for a wide range of Δ. Rejection of a disturbance to Θ is even better (i.e., the slope of $G(1, \Theta)$ is closer to 1), and the slack region extends to much higher values of Θ (the reason for this is outlined in Supplementary Section 2).

Closed Loop Stability. We can investigate the stability of the system in eq 1a−g by assuming that at equilibrium (which lies in mode m_0), each individual term in the equation for $\dot{p}$ is zero (i.e., $R_{off}, R_{on} \approx 0$). Linearizing about this point (in terms of D, z, z^*, I, and X) gives the Jacobian

$$\mathbf{J} = \begin{bmatrix} -\delta_2 & 0 & 0 & 0 & 0 \\ -\Theta p\alpha_1 & -\delta_1 - Kz^* & -Kz & 0 & 0 \\ 0 & -Kz^* & -\delta_1 - Kz & 0 & 0 \\ 0 & \Delta\beta_{I1} & \Delta\beta_{I2} & -\delta_2 & 0 \\ 0 & 0 & \Delta\beta_X & 0 & -\delta_2 \end{bmatrix} \tag{6}$$

which has eigenvalues $\lambda_{1,2,3} = -\delta_2$ and

$$\lambda_{4,5} = -\delta_1, -\delta_1 - K(z + z^*) \tag{7}$$

, and thus, all system poles (eigenvalues of eq 6) are in the left half plane, meaning this equilibrium is stable. We can numerically evaluate the eigenvalues for the complete system's Jacobian (i.e., including p in eq 6) about its equilibrium when $\Delta = \Theta = 1$, which returns (approximately) the same eigenvalues as above and an additional sixth value of $\lambda_6 = -4.4 \times 10^{-6}$

DOI: 10.1021/acssynbio.9b00125
ACS Synth. Biol. XXXX, XXX, XXX−XXX

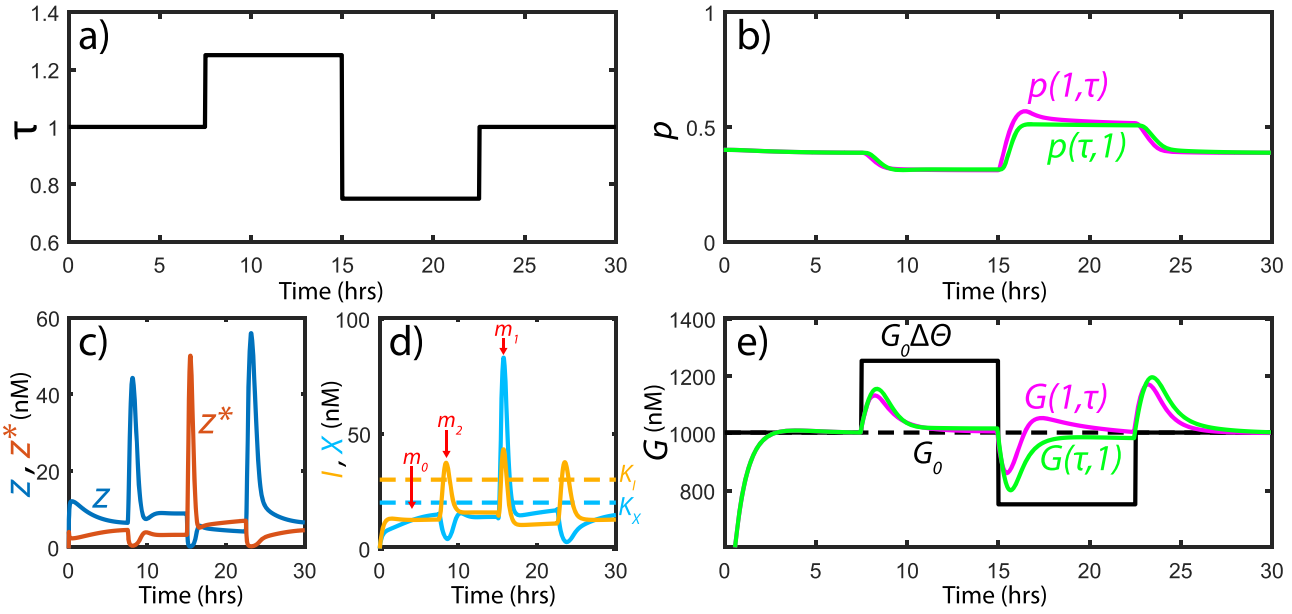

Figure 3. Dynamic simulation of disturbance rejecting behavior. (a) Disturbance profile τ substituted for Δ or Θ in subsequent subfigures. (b) The proportion of plasmids in their ON state (p) varies in response to disturbance in Δ ($G(\tau, 1)$) or Θ ($G(1, \tau)$). (c) The concentration of each mRNA species and (d) the concentration of I and X for $\Delta = \tau$, $\Theta = 1$. Spikes in concentration appear immediately following application of a disturbance, pushing the production rates of z and z^* out of balance. Example points at which the system is in each of its operating modes $m_{0,1,2}$ are labeled. (e) System output G, demonstrating near-perfect rejection of disturbance to either Δ or Θ. $G_0\Delta\Theta$ indicates the system's expected steady-state output if no control system was in place.

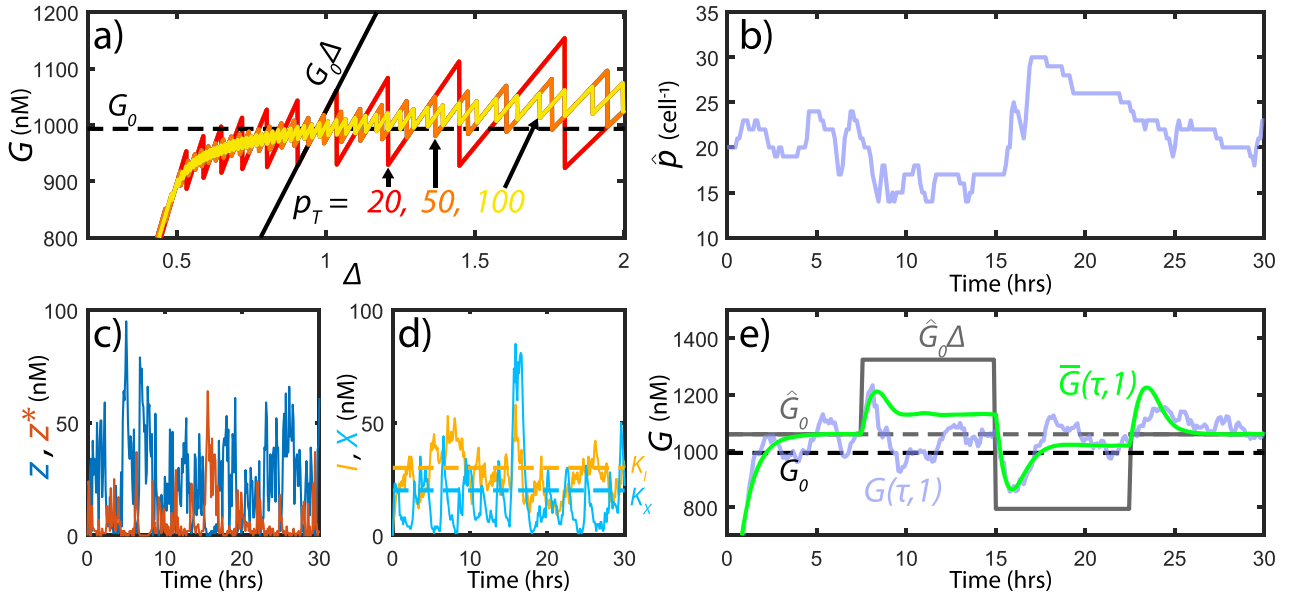

Figure 4. Stochastic simulation of disturbance rejecting behavior. (a) The dependence of our system's behavior on the copy number of DNA registers (p_T) simulated as described in the text. Other quantities plot parallel those in Figure 2b. (b–d) Similar to Figure 3b–d but for a single stochastic simulation run and with $\Theta = 1$. In panel b, the total number of ON registers ($\hat{p}$) is plotted, rather than the ON proportion of total registers (p). (e) System output G for a single stochastic simulation ($G(\tau, 1)$) and the average output of 3000 stochastic simulations ($\bar{G}(\tau, 1)$). The target output (mean steady-state G value when $\Delta = 1$) for the stochastic case ($\hat{G}_0$) differs to that for the deterministic case (G_0, see Figure 3e) as described in the text.

(corresponding to the slower, stable time scale), which is as expected much smaller than δ_2 (previously the eigenvalue of smallest magnitude).

Dynamic Simulation. In Figure 3, we numerically integrate the system in eq 1a–g, applying a time-varying disturbance profile $\tau(t)$ (Figure 3a) to Δ (with $\Theta = 1$, $G(\tau, 1)$) and then to Θ (with $\Delta = 1$, $G(1, \tau)$). Following a step change in τ, the system rapidly varies p (Figure 3b), which is driven by fluctuating mRNA concentrations (Figure 3c), which govern expression of I and X (Figure 3d). We observe that the system is achieving the intended switching behavior: I and X concentrations spike for short periods of time, rapidly driving p close to its new equilibrium, and then remain below K_I and K_X, respectively. The system output (Figure 3e) converges close to its preadaptation level following each disturbance, though this occurs over a longer time scale, because protein G is assumed to be stable (δ_3 is small).

DOI: 10.1021/acssynbio.9b00125
ACS Synth. Biol. XXXX, XXX, XXX−XXX

Stochastic Simulation. Though in previous sections we have assumed that p is a continuous variable, in practice, a finite number of DNA registers will be present within a given cell (e.g., one, or perhaps a couple, per plasmid). We investigate the impact of discretising p by setting

$$\hat{p} = \text{round}(p \times p_T) \tag{8}$$

and then substituting $p = \hat{p}/p_T$ in eq 1a−g. Here p_T is the copy number (per cell) of the flippable DNA register, and the round function returns its argument rounded to the nearest integer. We solve eq 1a−g with this modification to find the steady-state value of G as Δ is varied in Figure 4a, observing that as p_T is increased, our system's output converges to the $p_T = \infty$ behavior (i.e., Figure 2b).

As our system operates in a regime where concentrations of some system species (namely, z and z^*) are low, the stochasticity of individual biochemical reactions may substantially influence its output. This phenomenon is frequently described as *intrinsic noise*,[33] as it represents variability introduced within a given system. In Figure 4b−e, we perform tau-leaping Gillespie simulations of the system, setting $p_T = 50$ cell^{-1} and expressing each state variable in terms of integer copies per cell (rather than concentration). This follows from an average *E. coli* cell volume of 0.6 μm^3, meaning that a 1 nM concentration corresponds to approximately 1 molecule per cell. We observe substantial variability in z and z^* concentrations (Figure 4c), which drives variability in I and X (Figure 4d) and through that $\hat{p}$ (Figure 4b) and ultimately G (Figure 4e). In Figure 4e, we observe that stochastic treatment of this system increases its mean output level (from G_0 to $\hat{G}_0$) and (as an average of many simulations, $\overline{G}$) degrades the accuracy of adaptation to changing Δ. This changed behavior arises due to the time-averaged value of Kzz^* in eq 1b,c being reduced in the stochastic case. This intuitively follows from the fact that $\mathbb{E}[zz^*] = \mathbb{E}[z]\mathbb{E}[z^*] + \text{cov}(z, z^*)$ (where $\mathbb{E}$ and cov are the expectation and covariance of a random variable, respectively), and their covariance will be negative (because of negative interdependence introduced by $-Kzz^*$), thus reducing the expected magnitude of the product zz^* (for further analysis of this situation, see refs 7 and 34).

DISCUSSION

Our results demonstrate that the proposed switching control architecture is able to effectively reject a wide range of disturbances to either translation or transcription rate. Similar switching controllers are employed in traditional engineering situations when a controlled variable needs to be maintained close to a set-point and minimization of energy used for control actuation is also important.[30] For example, refrigeration/heating systems are often implemented by defining temperature limits above/below a set-point, outside of which the corresponding machinery is activated.[35] Such implementations can be highly efficient, because minimal energy is consumed when the temperature is in the slack region near to its set-point.[35] Analogously, for the biological controller outlined herein, the two DNA flipping operations represent cellular machinery, which is activated when the system leaves its slack region, and the consumption of energy (this time in the form of cellular resources) is minimal within the slack region.

Although Δ_p, Θ_p represent minimum disturbance limits that result in control saturation, the other limits described are solely constraints on the low-burden slack region, in which the controller is designed to operate. These can be exceeded without degrading control capability but come at the expense of increased protein production (and hence burden) in mode m_0. Tuning of system parameters would allow the system's set-point to be placed closer to the middle of this range. As Δ, Θ grow, the primary limit on the system's adaptative ability will thus be that imposed by the discretization of the DNA register state: p cannot be made arbitrarily small, and so, large Δ, Θ cause a stepped response (Figure 4a), particularly when the total number of DNA registers (p_T) is small. Furthermore, regulation of z by measurement protein species D may lose linearity (and saturate) for large Δ, Θ, providing an additional upper limit on disturbance size. The system's adaptive capability was degraded when constituent reactions were simulated stochastically; this phenomenon has been demonstrated to depend upon a system's operating parameter regime[34] and thus would be a target for experimental parameter tuning. Our system's design is intended to minimize the burden it imposes on a host cell by operating in a state where I, X (and potentially D) protein concentrations are small. However, in doing so, trade-offs are being made in terms of consumption of different cellular resources. For example, maintaining a large number of DNA registers (p_T) within a cell may also impact growth and other cellular processes.

One challenge posed by experimental implementation of the proposed control system is the creation of mRNA species z and z^*, which encode genes and also bind to one another. Similar behaviors have been observed in some natural systems,[36] though are at present beyond the capabilities of commonly used RNA engineering tools. In Supplementary Section 3, we analyze an analogous architecture, in which each mRNA is coexpressed with a repressing sRNA (and thus z and z^* do not need to mutually bind). The design of each mRNA is thereby simplified, though tuning of sRNA binding strength (demonstrated in a number of recent synthetic biological studies[26,27,37]) is required instead.

Future work will include further stochastic analysis of the proposed control architecture's behavior as well as investigation of its parameter sensitivity. Experimental implementation would then likely require tuning of system parameters that are identified as being major determinants of performance, for example, via ribosome binding site variation or inclusion of protein degradation tags (i.e., to vary δ_2) as was done in past implementations of integrase/excisionase controllers.[24] In the broader sense, control mechanisms that utilize integrase/excisionase mediated DNA flipping may present interesting opportunities for low-burden (though some plasmid replication is required) dynamic information storage: Although information stored in the concentration of a protein (or phosphorylation state of a substrate) is diluted over time, the mean state of a DNA sequence is maintained (because it is copied in its present form). Future work may thus include development of different control schemes based upon the fundamental philosophy described herein, eventually leading to low-burden adaptive controllers with a diversity of synthetic biological applicatons.[3]

ASSOCIATED CONTENT

Supporting Information

The Supporting Information is available free of charge on the ACS Publications website at DOI: 10.1021/acssynbio.9b00125.

Supplementary Section 1: Parameter values used in simulations; Supplementary Section 2: Analysis of steady-state response to variation in Δ or Θ; Supple-

DOI: 10.1021/acssynbio.9b00125
ACS Synth. Biol. XXXX, XXX, XXX−XXX

mentary Section 3: Approximating mRNA−mRNA annihilation junctions using sRNA (PDF)

AUTHOR INFORMATION

Corresponding Authors

*E-mail: antonis@eng.ox.ac.uk.
*E-mail: harrison.steel@eng.ox.ac.uk.

ORCID

Antonis Papachristodoulou: 0000-0002-3565-8967

Author Contributions

H.S. concieved the idea and performed simulations. H.S. and A.P. wrote the manuscript.

Funding

H.S. is supported by the General Sir John Monash Foundation. A.P. is supported by EPSRC project EP/M002454/1.

Notes

The authors declare no competing financial interest.

ACKNOWLEDGMENTS

The authors would like to thank Yili Qian, Theodore Grunberg, and Christian Cuba Samaniego for discussion and advice relating to the ideas presented herein.

REFERENCES

(1) Del Vecchio, D., Dy, A. J., and Qian, Y. (2016) Control theory meets synthetic biology. *J. R. Soc., Interface 13* (120), 20160380.

(2) Steel, H., Lillacci, G., Khammash, M., and Papachristodoulou, A. (2017) Challenges at the Interface of Control Engineering and Synthetic Biology. *Proc. IEEE Conf. Decision Control*, 1014−1023.

(3) Khammash, M. (2016) An engineering viewpoint on biological robustness. *BMC Biol. 14* (1), 22.

(4) Yi, T. M., Huang, Y., Simon, M. I., and Doyle, J. (2000) Robust perfect adaptation in bacterial chemotaxis through integral feedback control. *Proc. Natl. Acad. Sci. U. S. A. 97* (9), 4649−53.

(5) El-Samad, H., Goff, J. P., and Khammash, M. (2002) Calcium homeostasis and parturient hypocalcemia: An integral feedback perspective. *J. Theor. Biol. 214* (1), 17−29.

(6) Steel, H., and Papachristodoulou, A. (2018) Design Constraints for Biological Systems that Achieve Adaptation and Disturbance Rejection. *IEEE Trans. Control Network Syst. 5* (2), 807−817.

(7) Briat, C., Gupta, A., and Khammash, M. (2016) Antithetic Integral Feedback Ensures Robust Perfect Adaptation in Noisy Biomolecular Networks. *Cell Syst. 2* (1), 15−26.

(8) Aoki, S. K., Lillacci, G., Gupta, A., Baumschlager, A., Schweingruber, D., and Khammash, M. (2019) A universal biomolecular integral feedback controller for robust perfect adaptation. *Nature 570*, 533.

(9) Hsiao, V., De Los Santos, E. L. C., Whitaker, W. R., Dueber, J. E., and Murray, R. M. (2015) Design and implementation of a biomolecular concentration tracker. *ACS Synth. Biol. 4* (2), 150−161.

(10) Annunziata, F., Matyjaszkiewicz, A., Fiore, G., Grierson, C. S., Marucci, L., Di Bernardo, M., and Savery, N. J. (2017) An Orthogonal Multi-input Integration System to Control Gene Expression in Escherichia coli. *ACS Synth. Biol. 6* (10), 1816−1824.

(11) Qian, Y., and Del Vecchio, D. (2018) Realizing integral control' in living cells: how to overcome leaky integration due to dilution? *J. R. Soc., Interface 15* (139), 20170902.

(12) Ang, J., and McMillen, D. R. (2013) Physical constraints on biological integral control design for homeostasis and sensory adaptation. *Biophys. J. 104* (2), 505−515.

(13) Samaniego, C. C., and Franco, E. (2017) An ultrasensitive motif for robust closed loop control of biomolecular systems. *Proc. IEEE Conf. Decision Control*, 5334−5340.

(14) Qian, Y., Huang, H. H., Jiménez, J. I., and Del Vecchio, D. (2017) Resource Competition Shapes the Response of Genetic Circuits. *ACS Synth. Biol. 6* (7), 1263−1272.

(15) Darlington, A. P., Kim, J., Jiménez, J. I., and Bates, D. G. (2018) Dynamic allocation of orthogonal ribosomes facilitates uncoupling of co-expressed genes. *Nat. Commun. 9* (1), 695.

(16) Dublanche, Y., Michalodimitrakis, K., Kummerer, N., Foglierini, M., and Serrano, L. (2006) Noise in transcription negative feedback loops: simulation and experimental analysis. *Mol. Syst. Biol. 2*, 41.

(17) Ceroni, F., Algar, R., Stan, G. B., and Ellis, T. (2015) Quantifying cellular capacity identifies gene expression designs with reduced burden. *Nat. Methods 12* (5), 415−418.

(18) Liao, C., Blanchard, A. E., and Lu, T. (2017) An integrative circuithost modelling framework for predicting synthetic gene network behaviours. *Nat. Microbiol. 2*, 1658.

(19) Nystrom, A., Papachristodoulou, A., and Angel, A. (2018) A Dynamic Model of Resource Allocation in Response to the Presence of a Synthetic Construct. *ACS Synth. Biol. 7*, 1201−1210.

(20) McBride, C., and Del Vecchio, D. (2018) Resource Sensor Design for Quantifying Resource Competition in Genetic Circuits. *Proc. IEEE Conf. Decision Control*, 1865.

(21) Bonnet, J., Subsoontorn, P., and Endy, D. (2012) Rewritable digital data storage in live cells via engineered control of recombination directionality. *Proc. Natl. Acad. Sci. U. S. A. 109* (23), 8884−8889.

(22) Roquet, N., Soleimany, A. P., Ferris, A. C., Aaronson, S., and Lu, T. K. (2016) Synthetic recombinasebased state machines in living cells. *Science 353*, aad8559.

(23) Siuti, P., Yazbek, J., and Lu, T. K. (2013) Synthetic circuits integrating logic and memory in living cells. *Nat. Biotechnol. 31* (5), 448−52.

(24) Folliard, T., Steel, H., Prescott, T. P., Wadhams, G., Rothschild, L. J., and Papachristodoulou, A. (2017) A synthetic recombinase-based feedback loop results in robust expression. *ACS Synth. Biol. 6*, 1663.

(25) Agrawal, D. K., Tang, X., Westbrook, A., Marshall, R., Maxwell, C. S., Lucks, J., Noireaux, V., Beisel, C. L., Dunlop, M. J., and Franco, E. (2018) Mathematical Modeling of RNA-Based Architectures for Closed Loop Control of Gene Expression. *ACS Synth. Biol. 7*, 1219−1228.

(26) Kelly, C. L., Harris, A. W. K., Steel, H., Hancock, E. J., Heap, J. T., and Papachristodoulou, A. (2018) Synthetic negative feedback circuits using engineered small RNAs. *Nucleic Acids Res. 46*, 9875−9889.

(27) Huang, H.-H., Qian, Y., and Del Vecchio, D. (2018) A quasi-integral controller for adaptation of genetic modules to variable ribosome demand. *Nat. Commun. 9*, 5415.

(28) McCardell, R. D., Huang, S., Green, L. N., and Murray, R. M. (2017) Control of bacterial population density with population feedback and molecular sequestration, *bioRxiv*. https://www.biorxiv.org/content/10.1101/225045v1.

(29) Liberzon, D. (2003) *Switching in Systems and Control*, Springer.

(30) Morse, A. S. (1995) Control using logic-based switching. In *Trends in Control: A European Perspective* (Isidori, A., Ed.) pp 69−113, Springer.

(31) Bowyer, J. E., Hsiao, V., Wong, W. W., and Bates, D. G. (2017) Mechanistic modelling of a recombinasebased two-input temporal logic gate. *Eng. Biol. 1*, 40−50.

(32) Ferrell, J. E., and Ha, S. H. (2014) Ultrasensitivity part I: Michaelian responses and zero-order ultrasensitivity. *Trends Biochem. Sci. 39* (10), 496−503.

(33) Elowitz, M., Levine, A., Siggia, E., and Swain, P. (2002) Stochastic gene expression in a single cell. *Science 297* (5584), 1183−6.

(34) Olsman, N., Xiao, F., and Doyle, J. C. (2019) Architectural Principles for Characterizing the Performance of Antithetic Integral Feedback Networks. *iScience 14*, 277−291.

(35) Fayazbakhsh, M. A., Bagheri, F., and Bahrami, M. (2015) Gray-box model for energy-efficient selection of set point hysteresis in heating, ventilation, air conditioning, and refrigeration controllers. *Energy Convers. Manage. 103*, 459−467.

DOI: 10.1021/acssynbio.9b00125
ACS Synth. Biol. XXXX, XXX, XXX−XXX

(36) Thomason, M. K., and Storz, G. (2010) Bacterial Antisense RNAs: How Many Are There, and What Are They Doing? *Annu. Rev. Genet. 44* (1), 167−188.
(37) Na, D., Yoo, S. M., Chung, H., Park, H., Park, J. H., and Lee, S. Y. (2013) Metabolic engineering of Escherichia coli using synthetic small regulatory RNAs. *Nat. Biotechnol. 31* (2), 170−4.

DOI: 10.1021/acssynbio.9b00125
ACS Synth. Biol. XXXX, XXX, XXX−XXX